

Influence of eddy current losses in the optimization of linear coreless BLDC motors with PCB windings

Guillaume François, François Baudart, Bruno Dehez
Mechatronic, Electrical Energy, and Dynamic systems (MEED)
Institute of Mechanics, Materials and Civil Engineering (IMMC)
Université catholique de Louvain (UCL)
Louvain-la-Neuve, Belgium
g.francois@uclouvain.be, bruno.dehez@uclouvain.be

Abstract—This paper presents a series of numerical models aimed at estimating the main characteristics of linear coreless BLDC motors for the optimal sizing of these latter. The paper concentrates on windings printed on PCB. This kind of winding offers opportunities to significantly improve motors' performance, although it is more subject to eddy current losses than wire windings. Therefore, considering the harmonics contained in the airgap magnetic field, the work especially focus on the development of a 2D FEM model able to estimate these eddy currents in the copper tracks. The objective is to evaluate the eddy current harmonics and to adapt the winding shape and the motor dimensions, accordingly. The final aim of this work is therefore to propose full motor optimizations for various operating points and to observe the evolution of its optimal configuration.

Index Terms—Eddy currents, FEM, PCB winding, Optimizations, Operating speed, Losses, Linear, Coreless, BLDC.

I. INTRODUCTION

PCB (printed circuit boards) technology opens the way for new geometries and topologies of windings that result in more powerful and efficient slotless brushless DC (BLDC) motors. It has been demonstrated that the use of PCB can significantly increase their performance [1], [2]. This improvement comes from the ability to produce winding shapes and topologies that link more magnetic flux, while minimizing the electrical resistance and from the ability to adjust the width of the conductor along the track.

However, at high speed, the presence of eddy currents inside the copper tracks can wipe out the motor performance by generating extra losses [3], [4], [5]. Therefore, in order to ensure an optimal design, these losses have to be correctly evaluated and taken into account in the optimization process. For example, this will impact the width of the conductive tracks. Indeed, decreasing this latter strongly reduces the eddy current losses. As decreasing the width of the conductive track also increases the Joule losses through the electrical resistance, the optimal design should result from a trade-off. In addition, as the eddy current losses are linked to the

operating speed while the Joule losses depend on the supply current, the trade-off on the width of the conductive tracks will depend on the considered operating point.

In previous works, numerical and analytical models were proposed to evaluate the eddy current losses in a PCB winding. The models were applied to a single pole pair rotating machine taking into consideration only the unique fundamental component [3], [6]. In linear machines, the successive magnets disposed in alternate directions produce an airgap magnetic field with a large harmonic content [7]. Each of these harmonics generates eddy currents in the winding and it is therefore important to be able to take each of them into account during the optimal sizing process. In this paper this is done through a 2D frequential FEM model. This choice is motivated by the compromise it offers between the large computational efforts required for full 3D numerical models and the very poor accuracy of the analytical models when considering the harmonics.

Within this context, this paper proposes electric, magnetic and thermal models of a linear coreless BLDC motor with airgap PCB winding. Then, thanks to these models, full motor design optimizations are performed at various operating points. The optimal configuration search is done under the constraint of a fixed limited amount of power losses. The winding shape, the conductor track width and the internal motor thicknesses are adapted to maximize the force developed by the mover. In addition to these variables, the pole pitch and the magnet pitch factor are also released in order to possibly modulate the harmonic content of the airgap magnetic field. Finally, a comparison is made between the dimensional characteristics of the machines obtained through multiple optimizations.

The remainder of this paper is organized as follows. Section II describes the linear motor and its parameterization. Section III presents the models required for the motor sizing. Section IV describes the optimization problem, including the objective function, the constraints and the optimization variables. Eventually, section V discusses the results.

G. François is a FRIA Grant Holder of the "Fonds de la Recherche Scientifique"-FNRS, Belgium.

II. MOTOR DESCRIPTION & PARAMETERIZATION

The study case is a linear coreless BLDC motor as depicted in Fig.1.

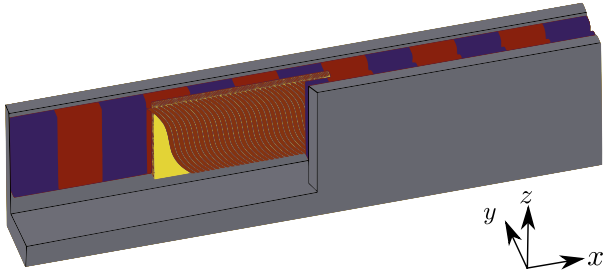


Fig. 1. Representation of the linear BLDC motor.

The mover is composed of a multi-layer tri-phases winding printed on PCB and inserted into a U-shape stator with permanent magnets (PM) on both sides. The magnets are magnetized perpendicularly to the mover plane and are successively disposed in alternate directions. The winding is overlapping and distributed along the mover with a pole pitch equal to the stator pole pitch τ . The topology of the winding corresponds to the infinity shape proposed in [8] and depicted in Fig. 2 and 3.

The internal dimensions of the motor are introduced in Fig. 4. As for the winding, it is approximated by n linear segments s_i whose end points (x_{i-1}, z_{i-1}) and (x_i, z_i) become the parameters characterizing the winding shape. Thanks to the symmetries, only a quarter of loop needs to be considered [6], [8]. A complete winding is composed of N_l double faced layers. On each of these layers, there are p_w number of poles, and each pole contains N_t number of loops.

Finally, providing that the end-windings area does not contribute to the torque, the electrical resistance is reduced by shortening the conductor tracks as shown in Fig. 3. Furthermore, this simple geometric construction from the initial reference track also allows for simpler connections of the winding layers.

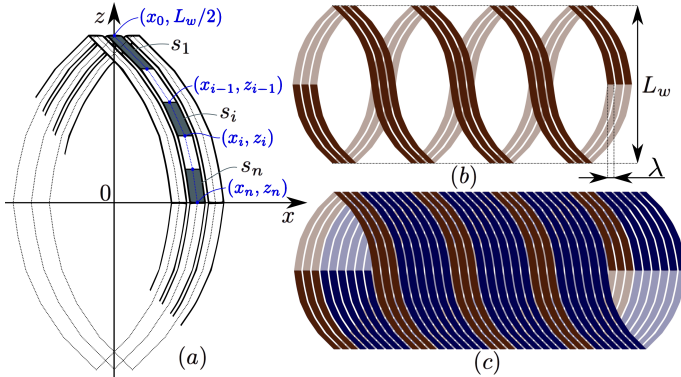


Fig. 2. (a) Winding parameterization; (b) Repetition of the reference loop to draw a complete phase and (c) eventually the full winding. Opaque and translucent segments respectively represent the top and the bottom tracks.

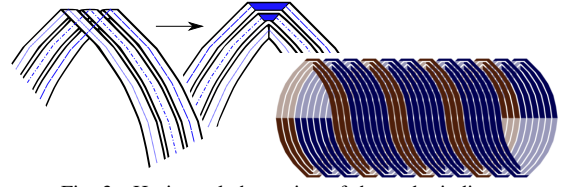


Fig. 3. Horizontal shortening of the end-windings.

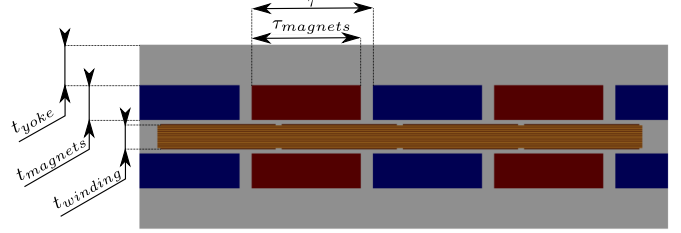


Fig. 4. Top view of the motor and definition of its internal dimensions.

III. MOTOR MODELING

In order to properly size the motor, it is generally needed to evaluate its force constant k_f and phase electrical resistance R_{ph} as they respectively link the force and the Joule losses P_{Joule} to the armature current. In slotless machines, and even more when using PCB winding instead of wire winding, it is also necessary to estimate the eddy current losses P_{eddy} as they may quickly become as important as the Joule losses at high speed. This section proposes models allowing to estimate k_f , R_{ph} and P_{eddy} . All of them use the finite element method in 2D domains which are meshed with triangles. The finite elements are of the first order and the formulations are solved in the Onelab [9] environment which implements the mesher *Gmsh* [10] and the solver *GetDP* [11].

A. Force constant

In linear machines, the force constant amplitude k_f is linked to the amplitude of the back-emf constant k_e by the following relation:

$$k_f = \frac{\sqrt{6}}{2} k_e \quad (1)$$

The back-emf constant itself corresponds to the amplitude of the flux variation perceived by a phase. Noting x_m the linear position of the mover, defined as the distance between the first loop of a phase and the magnetic axis of a north pole at the stator, we make the assumption that the flux $\Psi_j(x_m)$ embraced by a loop j is sinusoidally dependent on x_m :

$$\Psi_j(x_m) = \bar{\Psi}_j \cos\left((x_m - \Delta x_j) \frac{\pi}{\tau}\right) \quad (2)$$

where $\Delta x_j = (j-1)\tau/N_t$ is the position shift of loop j relatively to the first one. Combining (1) and (2), we have:

$$k_f = \frac{\sqrt{6}}{2} N_l \sum_j \left| \frac{\partial \Psi_j(x_m)}{\partial x} \right| = \frac{\sqrt{6} \pi}{2 \tau} N_l \sum_j \bar{\Psi}_j \quad (3)$$

Actually, the flux linked by a loop is given by:

$$\Psi_j(x_m) = \iint_{S_j} \mathbf{b}_0(x_m) \cdot \mathbf{dS} \quad (4)$$

where \mathbf{b}_0 is the magnetic flux density produced by the permanent magnets and S_j is the surface defined by the loop j .

Noting \mathbf{b}_s the remanent field of the magnets, one can find \mathbf{b}_0 by solving the non-linear *Magnetostatic's* equations. The magnetic permeability μ depends on the magnetic field \mathbf{h}_0 through the anhysteretic curves of the materials.

$$\begin{cases} \nabla \times \mathbf{h}_0 = 0 \\ \nabla \cdot \mathbf{b}_0 = 0 \\ \mathbf{b}_0 = \mu \mathbf{h}_0 + \mathbf{b}_s \end{cases} \quad (5)$$

In order to reduce this problem to a single-equation to be solved, a vector potential \mathbf{a}_0 is defined such that $\mathbf{b}_0 = \nabla \times \mathbf{a}_0$ and the above equations are combined as follows:

$$\nabla \times (\mu^{-1} \nabla \times \mathbf{a}_0) = \nabla \times (\mu^{-1} \mathbf{b}_s) \quad (6)$$

In order to keep a reduced computational effort, the 3D end effects are neglected and the motor is cut perpendicularly to the z axis to solve the problem in only a 2D domain. Inside this cut, the magnetic field is assumed to have non-zero components exclusively in the $x-y$ plane, and therefore the vector potential itself has only a single component z which is non-zero. Consequently, by defining the magnetic reluctivity $\nu = \mu^{-1}$, we have one single scalar equation to solve:

$$\begin{aligned} \nu \left(\frac{\partial^2 a_z}{\partial x^2} + \frac{\partial^2 a_z}{\partial y^2} \right) + \frac{\partial \nu}{\partial x} \frac{\partial a_z}{\partial x} + \frac{\partial \nu}{\partial y} \frac{\partial a_z}{\partial y} = \\ \nu \left(\frac{\partial b_{sx}}{\partial y} + \frac{\partial b_{sy}}{\partial x} \right) + \frac{\partial \nu}{\partial y} b_{sx} + \frac{\partial \nu}{\partial x} b_{sy} \end{aligned} \quad (7)$$

B. Electrical resistance

The electrical resistance is obtained using exactly the same approach as in [6]. A voltage difference V is applied at both ends of a loop's quarter and the resulting current is measured. The latter is obtained by solving an *Electrokinetics* problem:

$$\begin{cases} \nabla \times \mathbf{e} = 0 & \mathbf{n} \times \mathbf{e}|_{\Gamma_{input}, \Gamma_{output}} \\ \nabla \times \mathbf{h} = \mathbf{j} & \mathbf{n} \cdot \mathbf{j}|_{\Gamma_{lateral}} \\ \mathbf{j} = \sigma \mathbf{e} \end{cases} \quad (8)$$

where \mathbf{e} , \mathbf{j} and \mathbf{h} are respectively the electrical field, the current density and the magnetic field. Γ is the track frontier and $\mathbf{n} = (n_x, n_y)$ its normal. Because there is no magnetic field variation, the electrical field can be expressed thanks to a scalar potential $\mathbf{e} = -\nabla v$. Considering the tracks as infinitely thin, the problem becomes 2D and the above equations can be combined to obtain the following equation which has to be solved inside the conductors:

$$\sigma \left(\frac{\partial^2 v}{\partial x^2} + \frac{\partial^2 v}{\partial z^2} \right) + \frac{\partial \sigma}{\partial x} \frac{\partial v}{\partial x} + \frac{\partial \sigma}{\partial z} \frac{\partial v}{\partial z} = 0 \quad (9)$$

In the area of the horizontal shortenings, the bottom and the top conductive tracks are connected in parallel. In view of

considering this topology, while keeping the model in a planar domain, the existing electrical conductivity of the shortenings has been virtually doubled. Furthermore, the electrical resistance of each loop must be computed independently, since the add of these shortenings differentiates their shapes.

Eventually, the index j indicating the loop considered, the current density on a loop's quarter can be integrated so that:

$$I_j = \int_{\Gamma_{input,j}} \sigma \left| \frac{\partial v_j}{\partial x} n_x + \frac{\partial v_j}{\partial y} n_y \right| d\Gamma_{input,j} \quad (10)$$

this allows, p_w being the number of poles in the mover, to get the phase resistance:

$$R_{ph} = 4p_w N_l \sum_j \frac{V}{I_j} \quad (11)$$

C. Eddy current losses

In order to evaluate the eddy current losses in the conductors, caused by their displacement in front of the stator PM magnetic field, the assumptions proposed in [3] are as follows:

- The induced currents are assumed to be constant over the thickness of the copper track conductor, and have only in-plane components;
- The inductive coupling of the successive conductors is assumed to be very low compared to the effect of the PM magnetic field.

From these hypotheses, it results that eddy currents can be independently studied in each half of a reference loop. In addition, in order to get rid of the third dimension of the problem, and also to reduce the domain of computation to the conductive part only, the magnetic field variation along the track thickness is neglected:

$$\frac{\partial \mathbf{h}}{\partial y} = 0 \quad (12)$$

Applying the curl operator on both sides of the Ampere equation, one gets:

$$\nabla \times \mathbf{h} = \mathbf{j} \quad (13)$$

$$\nabla \times \nabla \times \mathbf{h} = \nabla \times \mathbf{j} \quad (14)$$

$$\nabla(\nabla \cdot \mathbf{h}) - \nabla^2 \mathbf{h} = \nabla \times \mathbf{j} \quad (15)$$

From this last equation, using the Gauss law ($\nabla \cdot \mathbf{h} = 0$), the Faraday law ($\nabla \times \mathbf{e} = -\frac{\partial \mathbf{b}}{\partial t}$), the constitutive equation $\mathbf{j} = \sigma \mathbf{e}$ and the assumption (12), it turns up that:

$$\frac{\partial^2 h_y}{\partial x^2} + \frac{\partial^2 h_y}{\partial z^2} = \sigma \frac{\partial b_y}{\partial t} \quad (16)$$

We neglect the coupling between the PM magnetic field and the magnetic field induced by the current flowing in the conductors. Therefore, in the airgap, the induction b_y is:

$$b_y = \mu h_y + b_{0y} \quad (17)$$

this leads to the diffusion formulation in h_y :

$$\frac{\partial^2 h_y}{\partial x^2} + \frac{\partial^2 h_y}{\partial z^2} = \mu \sigma \frac{\partial h_y}{\partial t} + \sigma \frac{\partial b_{0y}}{\partial t} \quad (18)$$

The source field due to the magnets, which is obtained thanks to a static simulation, can be decomposed into spatial harmonics:

$$b_{0y}(x) = \sum_{n=-\infty, \text{odd}}^{\infty} c_n e^{jn \frac{\pi}{\tau} x} \quad (19)$$

where j is the imaginary number and c_n the Fourier coefficients. In order to obtain a time dependent source term, accounting for the speed v of the mover, the static solution (19) is adapted accordingly:

$$b_{0y}(x, t) = \sum_{n=-\infty, \text{odd}}^{\infty} c_n e^{jn(\frac{\pi}{\tau} x - \frac{\pi}{\tau} x_m)} = \sum_{n=-\infty, \text{odd}}^{\infty} \bar{b}_{0y}^n e^{-jn \frac{\pi v}{\tau} t} \quad (20)$$

Then, equation (18) being linear, it can be solved independently for each harmonic n . Therefore, in the frequential domain, if we note:

$$h_y^n(x, t) = \Re(\bar{h}_y^n(x) e^{-jn \frac{\pi v}{\tau} t}) \quad (21)$$

the reaction field due to the n^{th} harmonic of the source, equation (18) becomes:

$$\frac{\partial^2 \bar{h}_y^n}{\partial x^2} + \frac{\partial^2 \bar{h}_y^n}{\partial z^2} - jn \frac{\pi v \mu \sigma}{\tau} \bar{h}_y^n = jn \frac{\pi v \sigma}{\tau} \sigma \bar{b}_{0y}^n \quad (22)$$

The eddy currents field generated by the n^{th} harmonic is therefore given by:

$$\mathbf{j}^n = \left(\frac{\partial \bar{h}_y^n}{\partial z}, 0, -\frac{\partial \bar{h}_y^n}{\partial x} \right) \quad (23)$$

and the mean losses associated are obtained as follows:

$$P_{eddy}^n = \frac{h_t}{\sigma} \iint \left(\frac{\partial \bar{h}_y^n}{\partial z} \right)^2 + \left(\frac{\partial \bar{h}_y^n}{\partial x} \right)^2 d\mathcal{A} \quad (24)$$

where \mathcal{A} and h_t are respectively the surface and the thickness of the conductor. Using the Parseval theorem, one can show that the mean in time of the total eddy current losses is simply the sum of the mean losses generated by each harmonic:

$$P_{eddy} = \sum_{n=1, \text{odd}}^{\infty} P_{eddy}^n \quad (25)$$

IV. MOTOR OPTIMIZATION

Considering that the motor can only dissipate a limited amount of power P_{diss} before its internal temperature reaches a threshold value, the optimization problem can be written:

$$\begin{cases} \max_{\chi} F(\chi) = k_f(\chi) \cdot I_{supply}(\chi) \\ \text{s.t. } P_{tot}(\chi) \leq P_{diss} \end{cases} \quad (26)$$

where F, χ, P_{tot} and I_{supply} are respectively the continuous force developed by the mover, the optimization variables, the total power dissipated and the DC current provided by the supply source.

Since only two kinds of losses are taken into account here, namely the Joules and eddy current losses, when the motor is

pushed to its maximum force use, the following equation can be written:

$$P_{tot} = P_{eddy} + P_{Joules} = P_{diss} \quad (27)$$

Therefore, the constraint on the total losses leads to a constraint on the supply current:

$$I_{supply} = \sqrt{\frac{P_{diss} - P_{eddy}}{2R_{ph}}} \quad (28)$$

and the optimization problem eventually becomes unconstrained:

$$\max_{\chi} k_f(\chi) \cdot \sqrt{\frac{P_{diss} - P_{eddy}(\chi)}{2R_{ph}(\chi)}} \quad (29)$$

V. RESULTS

For this study, we consider a moving part having a total length $p_w \cdot \tau$ and a total height L_w worth 60 mm and 30 mm respectively. The airgap thickness is set at 0.5 mm on both sides of the mover and the global thickness of the motor is limited to 23 mm. Five segments are used to draw the reference quarter of loop. A maximum of $P_{diss} = 15$ W has been imposed. Table I lists all the released variables when searching for the best machine configurations and their intervals of variation. To perform the optimizations, we used the NSGA-II algorithm from the Platypus python framework [12], [13].

TABLE I
OPTIMIZATION VARIABLES

Variable	Signification	Range
Winding shape		
λ	Azimuthal track width	0.2-2 mm
N_t	Number of loops per group	2-10
x_1, x_2, x_3, x_4	Positions of the s_i end points	$0 - \tau/2$
p_w	Number of mover poles	1-5
Internal thicknesses		
$t_{magnets}$	Thickness of the magnets	0.5-5 mm
$t_{winding}$	Thickness of the winding	0.5-5 mm
t_{yoke}	Thickness of the stator yoke	0.5-5 mm
$\tau_{magnets}$	Magnet width to pole pitch ratio	50-100 %

In order to ease the convergence of the optimization algorithm, a virtually non-integer number of poles is allowed. In Fig. 5, it can be observed that depending on the operating point it could lead to a non integer optimal number of poles. Obviously, in practice we should select the nearest integer.

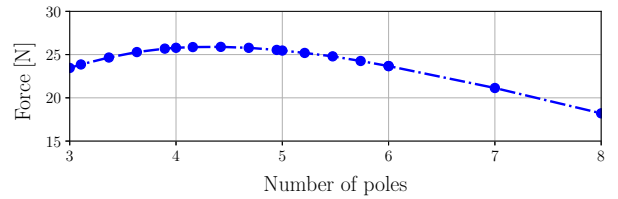


Fig. 5. Parametric analysis of the output force, varying the number of winding poles p_w of a motor initially optimized at $v = 4$ m/s.

A first result of the optimizations is that $\tau_{magnets}$ always tends to be 100%, which means that there is no modulation

of the magnetic field. In other words, it means that the reduction of the eddy current losses, that could be obtained by reducing the harmonic content, does not compensate for the increase of Joule losses needed to at least obtain the same output force. Indeed, reducing $\tau_{magnets}$ would also reduce k_f and therefore one must supply with more current to keep the same force level.

In Fig. 6, optimizations were performed taking into account, on the one hand, only the fundamental, i.e. $P_{eddy} = P_{eddy}^1$ and on the other hand, all the harmonics, i.e. $P_{eddy} = \sum_{n, odd} P_{eddy}^n$. Motors obtained considering only the fundamental were also re-evaluated using all the harmonics. The resulting curves suggest that both types of optimizations converge towards the same intrinsic optima, even if not taking into account the higher harmonics provides a falsely greater force as shown in Fig. 7. This suggestion is reinforced by Fig. 8, 9 and 10 which show respectively that the best configuration obtained for the internal thicknesses, the conductors width and the number of winding loops N_t is nearly the same with and without considering the higher harmonics. This can be partially explained by Fig. 11 showing that the ratio of each harmonic contribution to the total eddy current losses is kept constant and independent of the nominal speed. Besides, knowing these ratios at a certain speed, one could reconstruct the amplitudes at another speed by computing only a single harmonic contribution.

We also observed that the error made on the force estimation using only the fundamental, although small, increases with speed while the eddy current losses become more important. Again, this can be explained by Fig. 11 showing that, whatever the nominal speed considered, 20% of the losses is produced by the harmonics.

Figure 12 and 13 show that the speed does not significantly impact the optimal thicknesses inside the motor and the optimal number of poles respectively.

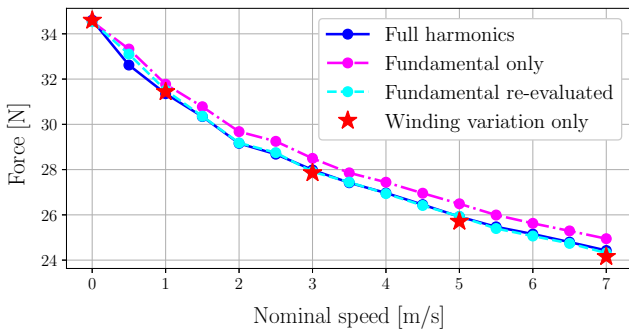


Fig. 6. Maximum continuous force developed by the motors, each resulting from an optimization, at various nominal speeds. In the case the optimization was not considering the impact of higher harmonics, the resulting motor has been re-evaluated using more harmonics. Stars represent the motor configuration obtained at 0 m/s for which only the track width and the number of loops have been adapted to optimize the motor.

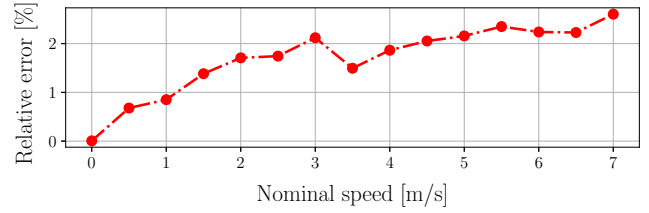


Fig. 7. Relative error on the force considering only the fundamental.

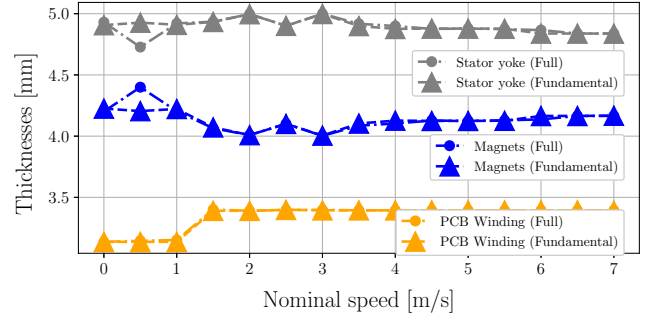


Fig. 8. Optimal thicknesses according to the desired speed, considering only the fundamental of the magnetic field or each of its harmonics.

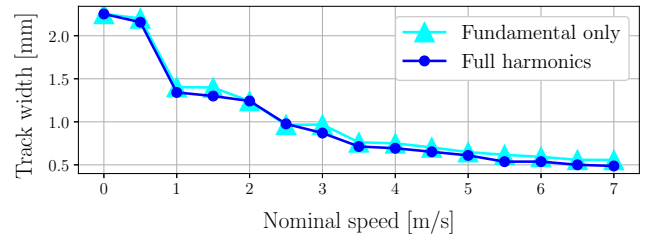


Fig. 9. Variation of the optimal track width regarding the desired nominal speed, considering higher harmonics of the magnetic field or not.

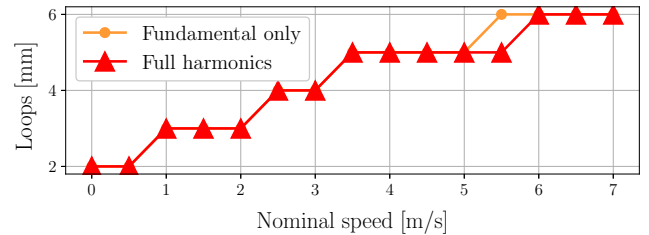


Fig. 10. Variation of the optimal number of loops N_t regarding the desired nominal speed, considering higher harmonics of the magnetic field or not.

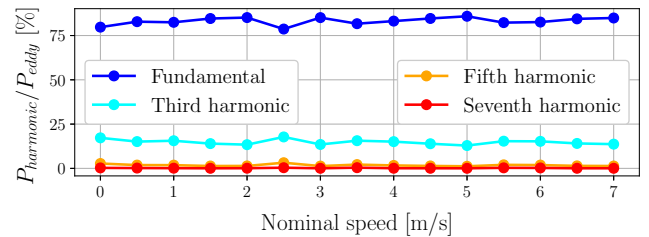


Fig. 11. Contribution of each harmonic in the total of the eddy current losses for the best motor configurations, at various nominal speeds.

Looking at the optimal winding shape in Fig. 14, one can observe that the number of loops increases accordingly with the speed while the track width decreases consequently. These evolutions can also be observed respectively in Fig. 9 and 10. This behavior can be explained by the fact that, at high speed, the eddy current losses are critical, so that the optimization reduces the conductor width by searching for a trade-off between minimizing the Joule losses through the phase resistance or minimizing the eddy current losses. Whereas at low speed, there are almost no eddy current losses and this simply tends to minimize the resistance.

Looking at the loop shape itself, it remains quite unchanged with the speed. This is also observed in Fig. 15 showing the relative positions of the points defining the reference loop quarter to build the winding. Indeed, they seem more or less invariant with the desired nominal speed.

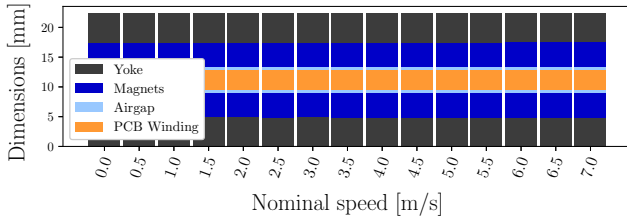


Fig. 12. Optimal space distributions resulting from the optimizations.

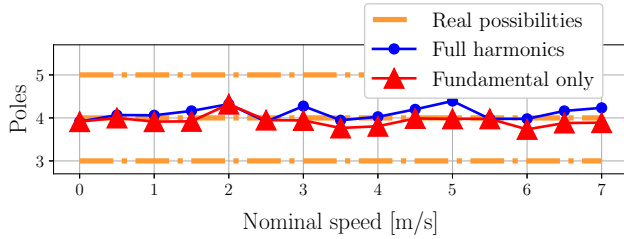


Fig. 13. Variation of the optimal number of poles p_w regarding the desired nominal speed, considering higher harmonics of the magnetic field or not.

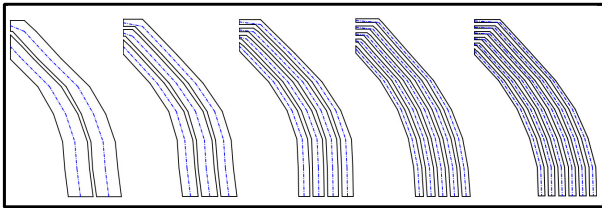


Fig. 14. From left to right, best configuration of the winding shape at 0 m/s, 1.5 m/s, 2.5 m/s, 4 m/s and 6 m/s.

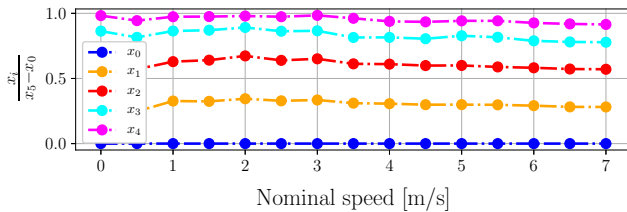


Fig. 15. Relative positions of the points describing the reference quarter of a loop to build the motor winding. The x_0 and x_5 correspond to the end points.

VI. CONCLUSION

In summary, it appears first that only the optimal number of loops and the optimal track width are impacted by the choice of a nominal speed, as demonstrated in Fig. 6. Consequently, one may first fully optimize a machine at an arbitrary speed then simply search for the best conductor width and the best number of loops when changing the desired speed. It also means that for a given motor, only the mover needs to be adapted if the required speed changes. A judicious choice for this first arbitrary speed would be zero. In this case, there are no losses except the Joules losses due to the supply current and then the objective function becomes:

$$k_f \cdot \sqrt{\frac{P_{diss}}{2R_{ph}}} \propto \frac{k_f}{\sqrt{2R_{ph}}} = k_m \quad (30)$$

where k_m is the motor constant, which is a comparison criterion independent of the external environment. Second, the results suggest that only the evaluation of the fundamental of the eddy current losses is required to obtain the optimal configuration of a motor. Third, the results have shown the importance of taking into consideration the harmonics in the evaluation of the eddy current losses to correctly estimate the output force. Therefore, even if it is possible to make do with a basic estimation of these harmonics, e.g., using a simple multiplicative factor, one cannot completely neglect them.

REFERENCES

- [1] B. Dehez, M. Markovic and Y. Perriard, "Theoretical and experimental investigation of flex-PCB airgap windings in slotless BLDC machines," 19th International Conference on Electrical Machines (ICEM), 2010.
- [2] F. Baudart, B. Dehez, J. Denies, M. Markovic, and Y. Perriard, "Shape optimization of flexible pcb slotless windings in bldc machines," International Conference on Electrical Machines and Systems, 2013.
- [3] G. François, F. Baudart, F. Henrotte and B. Dehez, "Numerical Investigation of Eddy Current Losses in Airgap PCB Windings of Slotless BLDC Motors," 2018 21st International Conference on Electrical Machines and Systems (ICEMS), Jeju, Korea (South), 2018, pp. 2702-2708.
- [4] A. Ahfock and D. Gambetta, "Stator eddy-current losses in printed circuit brushless motors," in IET Electric Power Applications, vol. 5, no. 1, pp. 159-167, January 2011.
- [5] N. J. Siakavellas, "Two simple models for analytical calculation of eddy currents in thin conducting plates," in IEEE Transactions on Magnetics, vol. 33, no. 3, pp. 2245-2257, May 1997.
- [6] G. François and B. Dehez, "Analytical estimation of eddy current losses in PCB winding for the optimal sizing of PM slotless motor," International Electric Machines & Drives Conference (IEMDC), San Diego, 2019. in press.
- [7] X. Liu, J. Gao, S. Huang and K. Lu, "Magnetic Field and Thrust Analysis of the U-Channel Air-Core Permanent Magnet Linear Synchronous Motor," in IEEE Transactions on Magnetics, vol. 53, no. 6, June 2017.
- [8] B. Dehez, F. Baudart and Y. Perriard, "Analysis of a new topology of flexible PCB winding for slotless BLDC machines," IEEE International Electric Machines and Drives Conference (IEMDC), Miami, FL, 2017.
- [9] ONELAB. 2019. URL: <http://onelab.info/wiki/ONELAB>.
- [10] C. Geuzaine and J.-F. Remacle, "Gmsh: a three-dimensional finite element mesh generator with built-in pre- and post-processing facilities," in International Journal for Numerical Methods in Engineering, 2009.
- [11] P. Dular, C. Geuzaine, F. Henrotte and W. Legros, "A general environment for the treatment of discrete problems and its application to the finite element method," in IEEE Transactions on Magnetics. Vol. 34, No. 5, pp. 3395-3398, Sept. 1998.
- [12] K. Deb, A. Pratap, S. Agarwal and T. Meyarivan, "A fast and elitist multiobjective genetic algorithm: NSGA-II," in IEEE Transactions on Evolutionary Computation, vol. 6, no. 2, pp. 182-197, April 2002.
- [13] Platypus framework. 2019. URL: <https://github.com/Project-Platypus>.